

# Mask as Supervision: Leveraging Unified Mask Information for Unsupervised 3D Pose Estimation

Yuchen Yang<sup>1,2\*</sup> Yu Qiao<sup>2</sup> Xiao Sun<sup>2†</sup>

<sup>1</sup>Fudan University <sup>2</sup>Shanghai Artificial Intelligence Laboratory

yangyc22@m.fudan.edu.cn {qiaoyu, sunxiao}@pjlab.org.cn

## Abstract

Automatic estimation of 3D human pose from monocular RGB images is a challenging and unsolved problem in computer vision. In a supervised manner, approaches heavily rely on laborious annotations and present hampered generalization ability due to the limited diversity of 3D pose datasets. To address these challenges, we propose a unified framework that leverages mask as supervision for unsupervised 3D pose estimation. With general unsupervised segmentation algorithms, the proposed model employs skeleton and physique representations that exploit accurate pose information from coarse to fine. Compared with previous unsupervised approaches, we organize the human skeleton in a fully unsupervised way which enables the processing of annotation-free data and provides ready-to-use estimation results. Comprehensive experiments demonstrate our state-of-the-art pose estimation performance on Human3.6M and MPI-INF-3DHP datasets. Further experiments on in-the-wild datasets also illustrate the capability to access more data to boost our model. Code will be available at <https://github.com/Charrrrrlie/Mask-as-Supervision>.

## 1. Introduction

Accurate 3D pose estimation plays a pivotal role in a myriad of domains, including human-computer interaction (HCI) [29, 56], robotics [13, 28, 36], sports performance analysis [45, 54], and augmented/virtual reality [9, 32]. However, acquiring annotated 3D data presents considerable challenges. While there are some multi-view databases [17, 33, 37] in controlled environments, obtaining labeled 3D data remains a costly, time-consuming, and labor-intensive process. Moreover, the quantity and diversity of 3D data, both in terms of appearance and motion,

\*Work performed during his internship at Shanghai Artificial Intelligence Laboratory.

†Corresponding author

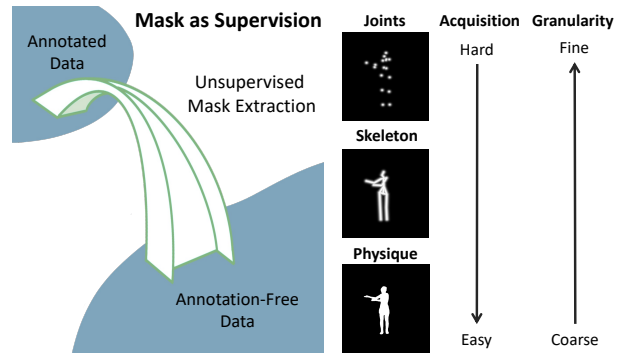


Figure 1. The schematic of mask as supervision. For unsupervised pose estimation, we aim to bridge the gap of annotations and utilize attainable data. Meanwhile, the foreground mask is easy to acquire and implies fine-grained information that motivates us.

are significantly inadequate. These limitations impede the generalization and robustness of 3D human pose estimation techniques when applied to novel environments.

To address the problem in 3D pose estimation, several methods attempt to predict 3D keypoints in an unsupervised manner. With no annotation required, it aims to effectively leverage vast data and impair the bias from particular human labeling to enhance the model’s ability in generalization and robustness. Generally, implicit [31, 58] and explicit [11, 14, 44, 48] human modeling from predicted keypoints are conducted. With background modeling or foreground masks, supervision can be provided by human reconstruction in the image. However, disregarding the interrelationship in human skeletons, the keypoints lack interpretability, requiring supervised post-processing (SPP) for conversion to human joints. Explicit modeling with human priors and geometric constraints offer feasibility in direct prediction in both 2D and 3D [19, 24, 25, 46]. Nonetheless, existing methods require unpaired annotations or manually designed templates, where human labor is still involved.

In this paper, we introduce a novel, unified approach for unsupervised 3D pose estimation that utilizes mask information, named Mask as Supervision. As depicted in Fig. 1,

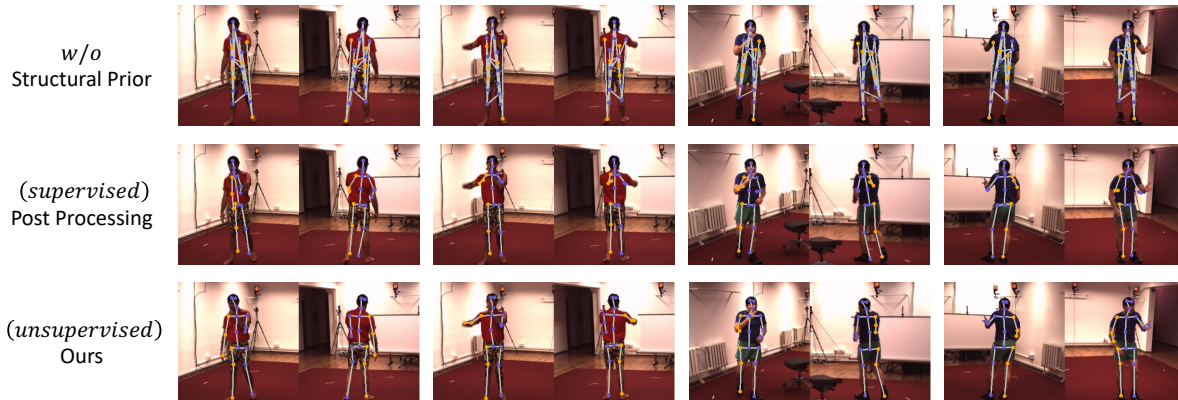


Figure 2. Different acquisition methods for structural priors. Known as an important prior, structural information leads to plausible skeletons in pose estimation. Without considering it, most previous methods necessitate supervised post-processing (SPP) during inference. To tackle this issue, we propose a method that enables effective and ready-to-use pose estimation in a fully unsupervised fashion.

our method is motivated by the recognition that the human body’s overall contour information possesses valuable insights. Particularly when extensive prior knowledge about the body shape is available, it provides rich clues for inferring the precise locations of 3D keypoints. Importantly, these informative contour cues can be obtained in an unsupervised manner by analyzing extensive video data and utilizing general segmentation algorithms.

To amplify the effectiveness and maximize the use of mask information, our proposed approach incorporates a range of techniques. These include a coarse-to-fine mask supervision method, defined using Skeleton and Physique Masks. As demonstrated in Fig. 2, it discovers body structure and shape priors to organize human skeletons and improve pose estimation accuracy. Furthermore, geodesic weighting and a cascaded optimization scheme are employed to estimate challenging distant keypoints with smooth solution space. To address the issue of left-right ambiguity, we adopt a robust strategy that effectively leverages a limited amount of unlabeled multi-view data.

Comprehensive experiments on Human3.6M [17] and MPI-INF-3DHP [33] datasets demonstrate that our method achieves superior performance among state-of-the-art unsupervised pose estimation methods. Additionally, our model possesses the capacity to leverage in-the-wild video data. Fine-tuning on TikTok dataset [18] without any kind of annotations, our model performs stronger generalization ability on unseen indoor and outdoor datasets.

Our contributions are summarised as follows:

- We present a novel proxy task that employs the mask as a unique supervisory signal for unsupervised 3D pose estimation. This task empowers us to efficiently harness an extensive collection of ‘in the wild’ data, leading to significantly enhanced performance.

- We introduce a set of well-established techniques, including the Skeleton and Physique Masks, Geodesic Weighting, and Cascaded Optimization. These techniques enable us to effectively extract valuable supervision from mask information by leveraging prior knowledge about the structure and shape of the human body.
- Without requiring supervised post-processing (SPP), our approach excels at predicting joints that hold physical interpretability. In the experiments, we demonstrate state-of-the-art performances in unsupervised pose estimation across widely-used datasets.

## 2. Related Work

**Unsupervised 2D Landmark Detection.** There have been plentiful methods [11, 19, 20, 31, 44, 58] focusing on discovering 2D keypoints in an unsupervised fashion. Generic supervision is human shape modeling from keypoints to reconstruct the image foreground. [19, 58] use Gaussian kernel to convert keypoints into heatmaps. [11, 20, 31] leverage articulation prior as part representations. However, those predicted keypoints show no inter-relationship in the human skeleton, and supervised post-processing techniques are necessitated to map them to labeled human joints. [41] designed a template to explicitly explain body shape. In that way, the post-processing can be removed while the template lacks generalization ability.

**Unsupervised 2D to 3D Lifting.** Lifting methods take 2D keypoints as input and obtain 3D joints. These studies assume that the 2D aspect of the pose has been previously given which does not strictly conform to the unsupervised 3D pose estimation settings. [23, 26, 53] constrain the network with geometric consistency by multi-view input or 3D rigid transformation. [4, 8, 57] utilize discriminator to pro-

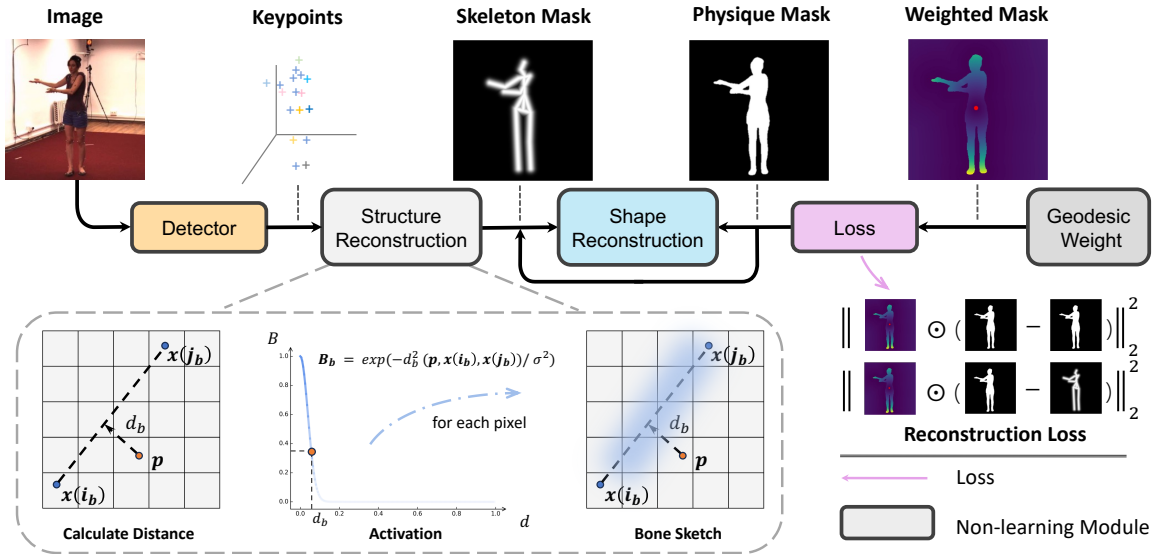


Figure 3. Overview. We aim to gain supervision from mask reconstruction for the 3D detector. The Skeleton Mask and the Physique Mask representations are proposed for reconstruction in a coarse-to-refine granularity. Additionally, Geodesic Weighting is adopted to further leverage mask information. Note that only the detector will be used during inference.

vide extra supervision from unpaired 2D keypoints.

**Unsupervised 3D Pose Estimation.** Learning 3D pose without annotation is a challenge that a few existing methods attempt to address. [14, 48, 50] extend 2D landmark discovery methods by leveraging multi-view constraints. Nevertheless, they still necessitate the supervised post-processing procedure. To obtain the interpretability in keypoints, it is vital to learn effective human priors to bridle the network. [24] utilizes human-designed template and unpaired 2D keypoints to represent priors. [46] takes skeleton map as 2D representation and constraint in 3D geometry while it also demands unpaired 2D annotations.

The closest setting to our method is [25], it adopts paired images with the same background and extracts texture and shape features from raw images and keypoints. It reaches unsupervised 3D pose estimation by applying a kinematic restriction in 3D and human prior from SMPL [30]. However, their results suffer from left-right ambiguity due to the lack of view constraints on the 2D mask representations.

As demonstrated later, our proposed method is fully unsupervised, requiring no annotations or templates, and effectively reduces left-right ambiguity.

### 3. Method

#### 3.1. 3D Pose Estimation from Single Images

We commence our discussion with a general formulation for the task of 3D human pose estimation from a single image.

Given an input image  $\mathbf{I}$ , our goal is to determine a set of joint locations  $\mathbf{X} \in \mathbb{R}^{J \times 3}$  in the 3D coordinate system,

$$\phi(\mathbf{I}) = \mathbf{X} \quad (1)$$

where  $J$  represents the number of joints as defined by the particular dataset in use. Typically, the  $\phi$  network is implemented via a backbone network [35], complemented by an underlying 3D heatmap representation. This heatmap subsequently predicts the 3D coordinates of the joints through an integral operation [49].

#### 3.2. Mask as Supervision

**Problem Definition.** For supervised learning, the ground truth joint locations  $\mathbf{X}^{\text{gt}}$  are provided. The backbone network is then optimized by minimizing the difference between these ground truth locations and the predicted positions, which is formally defined as the loss function  $L = \|\mathbf{X}^{\text{gt}} - \mathbf{X}\|_2^2$ . However, in unsupervised settings, the ground truth joint locations  $\mathbf{X}^{\text{gt}}$  are not available.

Motivated by various off-the-shelf unsupervised foreground mask extraction methods [3, 22, 27, 47], we assume that the **MASK** ground truth  $\mathbf{M}^{\text{gt}}$ , representative of the human form, is available and used as supervision for  $\mathbf{X}$  instead. Intuitively, one can regard  $\mathbf{M}^{\text{gt}}$  as a degraded version of  $\mathbf{X}^{\text{gt}}$  as depicted in Fig. 1.

As a result, **Mask as Supervision** can be defined as exploring a mask representation  $\mathbf{Z}$  that guides the pose estimator for effective training. Without loss of generality, we denote  $\mathbf{x}$  as the 2D counterpart of  $\mathbf{X}$ . It can be demonstrated

as

$$L_{Mask} = \|\mathbf{M}^{gt} - \mathbf{Z}(\mathbf{x})\|_2^2 \quad (2)$$

**Baseline.** A straightforward baseline is that all the predicted joints  $\mathbf{x}$  should lie within the confines of mask  $\mathbf{M}^{gt}$ . Concurrently, the joints  $\mathbf{x}$  should ideally envelop as much of  $\mathbf{M}^{gt}$  as possible. This yields a baseline mask representation that uses Gaussian kernel to interpret keypoints as follows,

$$\mathbf{Z}_{Base} = \mathbf{M}_{Gauss}(\mathbf{x}) \quad (3)$$

This simple baseline leads to a mass of ambiguities in the estimation. For example, interchanging any two keypoint locations in  $\mathbf{x}$  does not result in a variation in the loss value.

To address this issue, we propose leveraging prior knowledge concerning the human body’s *Structure* and *Shape* to mitigate erroneous predictions. As demonstrated in Fig. 3, this is achieved through two distinct representations: the *Skeleton Mask* and the *Physique Mask*, corresponding to structure and shape priors, respectively. These representations are deployed sequentially in a manner that transitions from coarse to refined granularity.

**Skeleton Mask from Body Structure Prior.** Keypoints on the human body do not exist independently; rather, they establish distinct interrelationships with articulated parts that collectively define the skeletal structure. This information aids in deriving the keypoints’ positions from the mask, with the consideration that the skeletal bones should also reside within the mask’s boundaries.

The body structure prior is formally defined as  $\mathbf{P} = \{(i_b, j_b) | b \in B\}$ , where  $i_b$  and  $j_b$  indicate the indices of the  $b$ th bone’s joints in  $\mathbf{x}$ , and there are  $B$  bones in total. It constrains the geometric relationships in keypoints since only specific ones are connected as bones.

The Skeleton Mask prediction is created by drawing a differentiable line segment with a specified width for each bone. Following the methods presented in [11, 12, 34], we implement this using an extended Gaussian distribution across the line segment. Each bone mask, denoted as  $\mathbf{B}_b$ , is formally defined as

$$\mathbf{B}_b(\mathbf{x}) = \exp(-d_b^2(\mathbf{p}, \mathbf{x}(i_b), \mathbf{x}(j_b))/\sigma^2) \quad (4)$$

where  $\sigma$  is a hyper-parameter controlling bone width, and  $d_b$  is the  $L_2$  distance between pixel  $\mathbf{p}$  in the map and the line segment defined by bone  $(\mathbf{x}(i_b), \mathbf{x}(j_b))$ .

We then merge all bone maps via pixel-wise summation to obtain the final Skeleton Mask  $\mathbf{M}_{Skel}(\mathbf{x}) = \sum_{b=1}^B \mathbf{B}_b(\mathbf{x})$ . The skeleton mask loss is defined as

$$L_{Skel} = \|\mathbf{M}^{gt} - \mathbf{M}_{Skel}(\mathbf{x})\|_2^2 \quad (5)$$

As demonstrated in the experiments, the structure prior effectively addresses the majority of ambiguity issues

within mask supervision. However, a gap still remains between the Skeleton Mask and the ground truth mask, resulting in the loss of fine details of the human body shape. The integration of a shape prior could further narrow this divergence, culminating in a more precise 3D pose estimation.

**Physique Mask from Body Shape Prior.** Several strategies exist for the integration of effective body shape priors. For instance, skinned models such as SMPL [30] could establish the transformational relationship between the 3D keypoints  $\mathbf{X}$  and the mesh vertices, and then form a more detailed Physique Mask  $\mathbf{M}_{Physo}$  by projecting the mesh points onto the image.

Even though this procedure can be rendered differentiable, their high non-linearity might complicate the system, making it prone to settling in local optima. Instead, we propose to directly regress the physique mask from the skeleton mask via a Shape Prior Network (SPN), denoted as  $\psi$ , and find it simple yet effective.

$$\mathbf{M}_{Physo}(\mathbf{x}) = \psi(\mathbf{M}_{Skel}(\mathbf{x})) \quad (6)$$

where  $\psi$  is implemented using a lightweight U-Net [40], and ended with a sigmoid activation [43] to make the pixel values in  $\mathbf{M}_{Physo}$  lie in  $(0, 1)$ . The physique mask loss is defined as

$$L_{Physo} = \|\mathbf{M}^{gt} - \mathbf{M}_{Physo}(\mathbf{x})\|_2^2 \quad (7)$$

The final objective is a weighted combination of both skeleton and physique mask losses.

$$\mathcal{L} = \lambda_s L_{Skel} + \lambda_p L_{Physo} \quad (8)$$

where  $\lambda_s$  and  $\lambda_p$  are hyper-parameters that balance the loss weights. At the initial stage of network optimization,  $\lambda_p$  is set to zero, as the  $L_{Skel}$  loss function can rapidly converge and eliminate the joint ambiguities. As  $L_{Skel}$  approaches convergence, the weight of  $\lambda_p$  gradually increases, thereby effectively incorporating the shape prior onto the Skeleton Mask and achieving a refinement effect.

### Geodesic Weighting for Hard Positives and Negatives.

It is well-established that joints further from the root on the kinematic tree are more challenging to estimate due to the increased variation [49]. Typically, these end joint positions appear in the mask’s locations that are distant from the centroid. Meanwhile, false positives lying on the background pixels should be unequally penalized according to the extent of deviation for smooth optimization. These insights motivate us to enhance the relevant hard positive and negative pixels on the mask ground truth  $\mathbf{M}^{gt}$ .

To this end, we employ geodesic distance [52] as a tool to augment the representation. The geodesic distance for

an entire image, denoted as  $\mathbf{G}$ , can be computed using the fast marching method [42], based on the mask. For the foreground, we initialize the mask centroid as zero point, while for the background, all mask pixels are set to zero points. The final Geodesic Weighting map is demonstrated in Fig. 3. Consequently, Eq. (8) can be modified as follows:

$$\mathcal{L} = \lambda_s \|\mathbf{G} \odot (\mathbf{M}^{\text{gt}} - \mathbf{M}_{\text{Skel}}(\mathbf{x}))\|_2^2 + \lambda_p \|\mathbf{G} \odot (\mathbf{M}^{\text{gt}} - \mathbf{M}_{\text{Physo}}(\mathbf{x}))\|_2^2 \quad (9)$$

Geodesic Weighting not only intensifies hard samples but also enhances the smoothness of the solution space, thus assisting in preventing convergence to local optima during the optimization process.

### 3.3. Leveraging Priors in Diverse Data Modalities

Up to this point, our framework has been discussed under the most widely applicable unsupervised single-image pose estimation setting. Next, we will demonstrate how the ‘‘Mask as Supervision’’ approach can be effectively integrated and enhanced with various modalities of data, by capitalizing on the modality-specific prior knowledge.

**Video Data Modality.** Video is the most common visual data modality apart from images. It is comprised of a series of consecutive frames, where adjacent frames imply spatial and temporal consistency. Therefore, basic background modeling algorithms [3, 7, 38] and the emerging unsupervised methods based on motion [5, 27] allow us to efficiently extract the foreground mask from video data.

**Multi-view Data Modality.** The presence of multi-view visual data is also increasingly noticeable in applications. Multi-view data offers 3D geometry constraints. Specifically, given  $n$  calibrated cameras, the geometric relations of 3D joints  $\mathbf{X}$  and its multi-view 2D counterparts  $\mathbf{x}^l$  are determined via direct linear transform [10] for triangulation.

$$\mathbf{X} = \Delta(\{\mathbf{x}^l\}_{l=1}^n, \{\mathbf{\Pi}^l\}_{l=1}^n) \quad (10)$$

where  $\Delta$  indicates triangulation operation.  $\mathbf{\Pi}^l = \mathbf{K}^l \mathbf{E}^l$  with camera calibration matrix  $\mathbf{K}$ ,  $\mathbf{E}$  given.

**Discussion: Ambiguity in Left-Right Reversal.** Owing to the symmetry of human body, using Masks as Supervision leads to a left-right reversal problem, also mentioned in [11, 41]. Networks may collapse that fail to distinguish the left and right side (i.e. all keypoints on the left of the image being treated as left joints) since both situations return the same error in the backward procedure.

In previous works, such as our Baseline in Eq. (3), the problem is neglected when introducing supervised post-processing (SPP) for evaluation. It utilizes annotations to

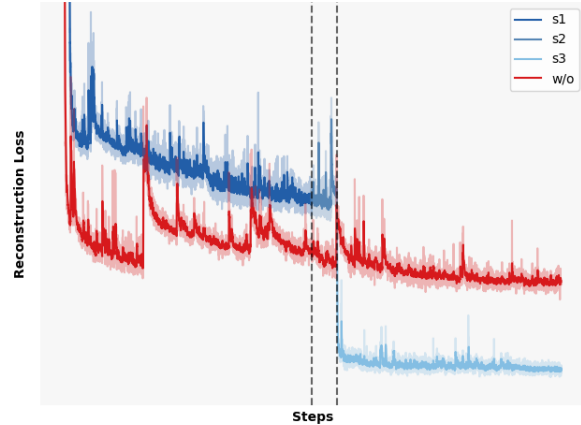


Figure 4. Reconstruction loss under different training strategies. The blue and red curves represent the cascade training and its absence, respectively. In addition, cascade stages are differentiated in colors. Losses are scaled for visualization.

train a linear or two hidden-layer network  $\theta : \mathbb{R}^{L \times 3} \rightarrow \mathbb{R}^{J \times 3}$  mapping high dimensional keypoints (usually  $L \geq 30$ ) to joints. Meanwhile, SPP makes it convenient to omit the processing of joint connectivity in their model design (further discussed in Sec. 4.6) while it leverages training set annotations thus not fully unsupervised.

In our framework, we adopt structure and shape prior to organizing human skeletons. To tackle the left-right reversal problem, we utilize the geometry constraints in Eq. (10) when multi-view data modality is accessible. The Skeleton Mask  $\mathbf{M}_{\text{Skel}}^l$  is sketched by the re-projected 2D keypoints  $\mathbf{x}_{prj}^l = \mathbf{\Pi}^l(\mathbf{X})$ . Only by eliminating ambiguity in prediction, networks can receive correct keypoints from triangulation and projection procedures.

### 3.4. Cascaded Optimization

The human skeleton exhibits a large diversity in various actions, containing priors in high dimensionality. It leads to multiple local optima during unsupervised optimization.

In the Mask as Supervision situation, it is simplistic to conceive how to locate the keypoints within the mask in a sub-optimal way. Without weakly supervised unpaired poses or laborious human-designed templates, we divide the optimization procedure into cascades with particular designs to avoid incorrect gradient decline paths. We demonstrate its effect in Fig. 4. With the cascade strategy, the model found a shortcut in the third stage while the model erroneously fell into a local optimum without such strategy.

Concretely, we only optimize the Skeleton Mask except for arms and hands for the first stage. It helps the network find a coarse location of each joint. As it gradually meets convergence, we then adopt the Shape Prior Network for joint optimization. Finally, arms and hands are taken

Table 1. Comparison with state-of-the-art methods on Human3.6M. **SPP**: supervised post-processing. **UP**: unpaired ground truth pose or its prior, **T**: manually designed template. **SF**: supervised flip to eliminate left-right ambiguity. † indicates our results do not consider the ambiguity in left-right reversal. †† indicates we do not consider inner skeleton relationships and follow the common SPP settings. The best results in SPP and No SPP groups are marked in red and blue. MPJPEs are in *mm*.

Method		Settings				Metrics (↓)			
		UP	T	SF	Joints	2D MSE-%	MPJPE	N-MPJPE	P-MPJPE
SPP	Thewlis <i>et al.</i> [51]	×	×	✓	2D	7.51	-	-	-
	Zhang <i>et al.</i> [58]	×	×	✓	2D	4.14	-	-	-
	Lorenz <i>et al.</i> [31]	×	×	✓	2D	2.79	-	-	-
	Suwajanakorn <i>et al.</i> [50]	×	×	×	3D	-	158.7	156.8	112.9
	Sun <i>et al.</i> [48]	×	×	×	3D	-	125.0	-	105.0
	Honari <i>et al.</i> [15]	×	×	✓	3D	-	100.3	99.3	74.9
	Honari <i>et al.</i> [14]	×	×	×	3D	<b>2.38</b>	73.8	72.6	63.0
SPP	Ours <sup>††</sup>	×	×	×	3D	2.52	<b>65.5</b>	<b>66.1</b>	<b>61.9</b>
No SPP	Schmidtke <i>et al.</i> [41]	×	✓	✓	2D	3.31	-	-	-
	Jakab <i>et al.</i> [20]	✓	×	✓	2D	<b>2.73</b>	-	-	-
	Sosa <i>et al.</i> [46]	✓	×	✓	3D	-	-	-	96.4
	Kundu <i>et al.</i> [24]	✓	✓	✓	3D	-	99.2	-	-
	Kundu <i>et al.</i> [25]	✓	×	✓	3D	-	-	-	89.4
No SPP	Ours <sup>†</sup>	×	×	✓	3D	3.17	<b>85.6</b>	<b>85.6</b>	<b>79.3</b>
	Ours	×	×	×	3D	3.63	95.9	96.8	90.4

into consideration, being supervised by both Skeleton and Physique Mask. The details can be found in the appendix.

## 4. Experiments

### 4.1. Datasets

We use the following datasets for training and evaluation. Note that, in the unsupervised setting, all ground truth poses are not accessible for our model during training.

**Human3.6M** [17]. Following [58], we select six activities (direction, discussion, posing, waiting, greeting, walking) and use subjects 1, 5, 6, 7, and 8 to train, subjects 9, and 11 to evaluate. 18 joints (add thorax) are predicted and compared with ground truth.

**MPI-INF-3DHP** [33]. Following [14], we use subjects 1 to 6 for training and subjects 7 and 8 for evaluation. We leave out the frames where the person is occluded. Evaluation joints are compatible with H36M.

**TikTok** [18]. It comprises single-view video sequences from social media with large appearance diversity, without any pose annotations. We select 42 sequences where most joints are visible and contain a single person.

**MPII** [2]. Images are collected in the wild with a single view. To evaluate the generalization ability of our model, we select the validation set for experiments.

### 4.2. Implementation Details

**Mask Extraction.** General segmentation methods are widely used to extract foreground masks from video data. Human3.6M dataset provides the foreground mask by the off-the-shelf graph cut algorithm [3]. MPI-INF-3DHP dataset adopts chroma key to extract masks in the motion capture environment with a green screen. [1] is utilized in TikTok dataset. With the help of the multi-prompt segmentation model, we select SAM [22] and obtain the mask with smooth and relatively accurate edges in our experiments.

**Training Details.** Experimentally, Batch Normalization [16] provides inaccurate batch statistics estimation during inference, leading to poor generalization capabilities in resolving ambiguities related to left-right reversal. Hence, we adopt Group Normalization [55] to replace Batch Normalization in our detector, which avoids parameter estimation during inference.

### 4.3. Quantitative Analysis

**Results on Human3.6M.** In Tab. 1, we compare against both 2D and 3D unsupervised pose estimation methods on the Human3.6M dataset. In previous studies, several laborious human-involved annotations or priors are introduced, which deviate from the strict definition of unsupervised learning. To ensure a fair comparison and clarify the experimental settings, we succinctly summarized them as follows:

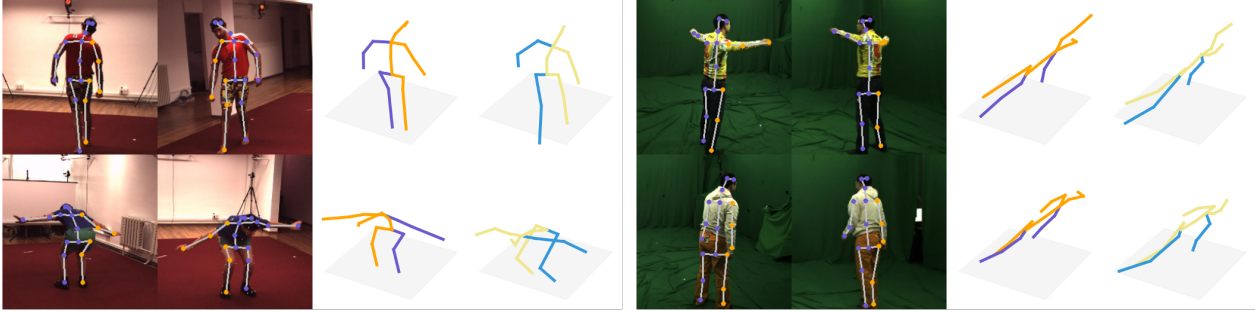


Figure 5. Qualitative results on Human3.6M and MPI-INF-3DHP datasets. We visualize joints in both 2D and 3D coordinate systems, for Human3.6M (left) and MPI-INF-3DHP (right) datasets. Every 4<sup>th</sup> column in each sub-figure shows 3D ground truth joints.

Table 2. Comparison with state-of-the-art methods on MPI-INF-3DHP. MPJPE is in *cm*. Note that the first four methods use supervised post-processing and Sosa *et al.* [46] uses unpaired 2D pose to obtain interpretable keypoints.

Method	PCK(↑)	AUC(↑)	MPJPE(↓)
Denton <i>et al.</i> [6]	-	-	22.28
Rhodin <i>et al.</i> [39]	-	-	20.24
Honari <i>et al.</i> [15]	-	-	20.95
Honari <i>et al.</i> [14]	-	-	14.57
Sosa <i>et al.</i> [46]	69.6	32.8	-
Ours	60.2	24.7	19.36
Ours (SPP)	<b>71.3</b>	<b>42.7</b>	<b>13.67</b>

SPP (supervised regression in post-processing), SF (supervised flip to eliminate left-right ambiguity), UP (unpaired pose or its prior), T (manually designed template).

Among these techniques, SPP (discussed in Sec. 3.3 and Sec. 4.6) relies entirely on 3D pose ground truth, which ignores the order and interrelationship of joints. Consequently, it requires separate consideration for comparison. In contrast, UP, T, and SF avoid directly utilizing annotations to construct skeleton structures but still rely on them to guide the learning or inference process, thus we mark them up accordingly.

On the contrary, our method is able to predict interpretable 3D joints without any annotation. Fairly, we also adopt SPP to alternate the skeleton mask. We outperform most methods in 2D and 3D metrics with or without the SPP procedure, showing state-of-the-art performances.

**Results on MPI-INF-3DHP.** With the aim to evaluate the performance on challenge scenarios, we conduct our model on MPI-INF-3DHP dataset [33], which involves a larger diversity of actions for further exploration. Tab. 2 presents our contestable performance with unpaired labels or SPP-necessitated methods. Detailly, without any kind of anno-

tations, we achieve advanced performance in MPJPE and considerable accuracy in PCK and AUC metrics. Note that not many unsupervised methods directly experiment on this challenging dataset. We demonstrate our results under the suggested PCK and AUC metrics in [33] calling for follow-up experiments.

#### 4.4. Qualitative Analysis

Qualitative results of keypoints predictions are shown in Fig. 5 for Human3.6M and MPI-INF-3DHP. We address the left-right reversal problem which lies in most mask-based unsupervised methods. Through a comparison of sub-figures both within and between them, our predictions demonstrate both intra-scene and inter-scene consistency, indicating that our model has the ability to handle different people and camera views while maintaining a consistent joint definition.

#### 4.5. Leveraging In-the-wild Data

Vast amounts of data from various sources are being generated, including real-world scenarios such as video sequences captured by a single camera. As a result, it is crucial and essential for unsupervised models that can effectively learn from in-the-wild data to enhance model robustness and generalization ability. Under our circumstances, our model possesses the ability to take single-view images as input, where the foreground masks can be extracted in the same way as multi-view video data.

To evaluate our model capacity of learning from in-the-wild data and to overcome the shortages of appearance diversity in mocap datasets, we conduct on TikTok dataset [18], which provides single-view videos without any pose annotations for view mix training. Formally, a fully initialized model on Human3.6M is chosen as the baseline. Then we train it on both Human3.6M and TikTok datasets, named Mixed-view Fine-tuning. For comparison, we take another strategy that merely uses Human3.6M data to train for the same epochs, named Multi-view Fine-tuning. We evaluate them on seen and unseen datasets, containing in-

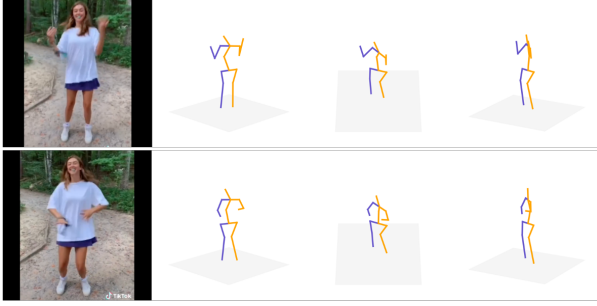


Figure 6. Qualitative results on TikTok dataset. We visualize the Mixed-view fine-tuning predictions in different views.

Table 3. Evaluations with different training strategies. MPJPEs are in *mm*. Note models are not trained on 3DHP [33] and MPII [2] datasets.

Settings	H3.6M MPJPE(↓)	3DHP PCK(↑)	MPII PCKh(↑)
Baseline	101.63	60.1	26.7
Multi-view ft	95.90	61.2	27.3
Mixed-view ft	94.82	63.4	28.1
<i>improvement</i>	<i>+1.08</i>	<i>+2.2</i>	<i>+0.8</i>

door and outdoor scenarios. The qualitative and quantitative results are demonstrated in Fig. 6 and Tab. 3.

It is insightful that Mix-view Fine-tuning surpasses Multi-view Fine-tuning in every metric, indicating the capability of absorbing in-the-wild data in our framework.

#### 4.6. Ablation Study

**Skeleton Mask as Structural Representation.** To verify the effectiveness of modeling structure prior, a simple way is to select the Baseline method in Eq. (3) that does not consider any human prior for a comparison.

As demonstrated in Fig. 2, the Baseline method in the first configurations fails to gain plausible skeletons due to the mass of ambiguity. Its optimization target is fitting keypoints within the mask and any interchange among keypoints will not lead to a fluctuation in the loss. In the second row, we show the capability of the post-process technique. With SPP, skeletal structures can be organized even without any extra designs. It is powerful but not fully unsupervised thus we leverage our effective unsupervised structure prior as the replacement.

Additionally, we adopt the Shape Prior Network  $\psi$  to ensure the structural prior knowledge is provided by the Skeleton Mask, rather than other proposed components. Quantitative results can be found in the appendix.

**Physique Mask as Shape Representation.** We leverage the physique mask to replenish the single representation from the skeleton mask approximating the ground truth mask. Hence we design several variations to discover the functionality of the physique mask in Tab. 4. The Shape Prior Network  $\psi$ , geodesic weighting  $\mathbf{G}$ , and triangulation  $\Delta$  are removed for baseline. Successively, those modules are rejoined into the framework for comparison. To demonstrate the results in eliminating left-right reversal ambiguity, we define an Ambiguity Ratio  $r$  as a metric.

$$r = \sum_{i=0}^D \min(f_i, N - f_i) / D \quad (11)$$

where  $f_i$  counts the times that keypoints adding the left-right flip gain less error in a scene with  $N$  camera views.  $D$  indicates the number of all evaluation samples.

Table 4. Ablation study on shape reconstruction.

Configurations	MPJPE (↓)	Ambiguity Ratio (↓)
<i>wo</i> $\psi$ , $\mathbf{G}$ , $\Delta$	118.1	48.73%
<i>wo</i> $\psi$ , $\mathbf{G}$	127.4	23.34%
<i>wo</i> $\mathbf{G}$	102.6	22.83%
Full	95.9	20.33%

Although without triangulation, the model gains better performance in MPJPE, it raises large ambiguity in left-right reversal according to our metric  $r$ .

#### 4.7. Limitations and Discussion

Our framework remains limited in a few aspects. Body occlusions carry ambiguity in the mask. Furthermore, inter-frame occlusions can be handled by learning from unobstructed samples while keypoints invisibility caused by frame cropping is still a challenge. Another limitation is human modeling. Currently, we consider all body parts articulated while fine-grained parts, such as the head area, do not satisfy this assumption. Upon that, fractional modeling may lead to further improvement.

### 5. Conclusion

We present an unsupervised 3D pose estimation framework that leverages unified mask information from structure and shape representations. The proposed model effectively organizes the human skeleton with priors from the mask, making it capable of providing interpretable keypoints and accessing annotation-free data. Performance on two widely used datasets demonstrates the superior ability of our model. Moreover, we illustrate the model can be enhanced by in-the-wild video data, by virtue of the fully unsupervised manner.



## Acknowledgement

This work is partially supported by the National Key R&D Program of China(NO.2022ZD0160100).

## References

- [1] <https://www.remove.bg/>. 6
- [2] Mykhaylo Andriluka, Leonid Pishchulin, Peter Gehler, and Bernt Schiele. 2d human pose estimation: New benchmark and state of the art analysis. In *IEEE Conference on Computer Vision and Pattern Recognition*, 2014. 6, 8
- [3] Yuri Boykov and Gareth Funka-Lea. Graph cuts and efficient nd image segmentation. *International Journal of Computer Vision*, 70(2):109–131, 2006. 3, 5, 6
- [4] Ching-Hang Chen, Amrith Tyagi, Amit Agrawal, Dylan Drover, Rohith Mv, Stefan Stojanov, and James M Rehg. Unsupervised 3d pose estimation with geometric self-supervision. In *Proceedings of the IEEE/CVF Conference on Computer Vision and Pattern Recognition*, pages 5714–5724, 2019. 2
- [5] Subhabrata Choudhury, Laurynas Karazija, Iro Laina, Andrea Vedaldi, and Christian Rupprecht. Guess what moves: Unsupervised video and image segmentation by anticipating motion. In *British Machine Vision Conference*, 2022. 5
- [6] Emily L Denton et al. Unsupervised learning of disentangled representations from video. *Advances in Neural Information Processing Systems*, 30, 2017. 7
- [7] Gianfranco Doretto, Alessandro Chiuso, Ying Nian Wu, and Stefano Soatto. Dynamic textures. *International journal of computer vision*, 51:91–109, 2003. 5
- [8] Kehong Gong, Jianfeng Zhang, and Jiashi Feng. Poseaug: A differentiable pose augmentation framework for 3d human pose estimation. In *Proceedings of the IEEE/CVF Conference on Computer Vision and Pattern Recognition*, pages 8575–8584, 2021. 2
- [9] DongHeun Han, RoUn Lee, KyeongMin Kim, and HyeongYeop Kang. Vr-handnet: A visually and physically plausible hand manipulation system in virtual reality. *IEEE Transactions on Visualization and Computer Graphics*, 2023. 1
- [10] Richard Hartley and Andrew Zisserman. *Multiple view geometry in computer vision*. Cambridge University Press, 2003. 5
- [11] Xingzhe He, Bastian Wandt, and Helge Rhodin. Autolink: Self-supervised learning of human skeletons and object outlines by linking keypoints. *Advances in Neural Information Processing Systems*, 35:36123–36141, 2022. 1, 2, 4, 5
- [12] Xingzhe He, Gaurav Bharaj, David Ferman, Helge Rhodin, and Pablo Garrido. Few-shot geometry-aware keypoint localization. In *Proceedings of the IEEE/CVF Conference on Computer Vision and Pattern Recognition*, pages 21337–21348, 2023. 4
- [13] Abdelfetah Hentout, Mustapha Aouache, Abderraouf Maoudj, and Isma Akli. Human–robot interaction in industrial collaborative robotics: a literature review of the decade 2008–2017. *Advanced Robotics*, 33(15-16):764–799, 2019. 1
- [14] Sina Honari and Pascal Fua. Unsupervised 3d keypoint estimation with multi-view geometry. *arXiv preprint arXiv:2211.12829*, 2022. 1, 3, 6, 7
- [15] Sina Honari, Victor Constantin, Helge Rhodin, Mathieu Salzmann, and Pascal Fua. Temporal representation learning on monocular videos for 3d human pose estimation. *IEEE Transactions on Pattern Analysis and Machine Intelligence*, 2022. 6, 7
- [16] Sergey Ioffe and Christian Szegedy. Batch normalization: Accelerating deep network training by reducing internal covariate shift. In *International Conference on Machine Learning*, pages 448–456. PMLR, 2015. 6
- [17] Catalin Ionescu, Dragos Papava, Vlad Olaru, and Cristian Sminchisescu. Human3.6m: Large scale datasets and predictive methods for 3d human sensing in natural environments. *IEEE Transactions on Pattern Analysis and Machine Intelligence*, 36(7):1325–1339, 2013. 1, 2, 6
- [18] Yasamin Jafarian and Hyun Soo Park. Learning high fidelity depths of dressed humans by watching social media dance videos. In *Proceedings of the IEEE/CVF Conference on Computer Vision and Pattern Recognition*, pages 12753–12762, 2021. 2, 6, 7
- [19] Tomas Jakab, Ankush Gupta, Hakan Bilen, and Andrea Vedaldi. Unsupervised learning of object landmarks through conditional image generation. *Advances in Neural Information Processing Systems*, 31, 2018. 1, 2
- [20] Tomas Jakab, Ankush Gupta, Hakan Bilen, and Andrea Vedaldi. Self-supervised learning of interpretable keypoints from unlabelled videos. In *Proceedings of the IEEE/CVF Conference on Computer Vision and Pattern Recognition*, pages 8787–8797, 2020. 2, 6
- [21] Diederik P Kingma and Jimmy Ba. Adam: A method for stochastic optimization. *arXiv preprint arXiv:1412.6980*, 2014. 2
- [22] Alexander Kirillov, Eric Mintun, Nikhila Ravi, Hanzi Mao, Chloe Rolland, Laura Gustafson, Tete Xiao, Spencer Whitehead, Alexander C. Berg, Wan-Yen Lo, Piotr Dollar, and Ross Girshick. Segment anything. In *Proceedings of the IEEE/CVF International Conference on Computer Vision*, pages 4015–4026, 2023. 3, 6
- [23] Muhammed Kocabas, Salih Karagoz, and Emre Akbas. Self-supervised learning of 3d human pose using multi-view geometry. In *Proceedings of the IEEE/CVF Conference on Computer Vision and Pattern Recognition*, pages 1077–1086, 2019. 2
- [24] Jogendra Nath Kundu, Siddharth Seth, Varun Jampani, Mugalodi Rakesh, R Venkatesh Babu, and Anirban Chakraborty. Self-supervised 3d human pose estimation via part guided novel image synthesis. In *Proceedings of the IEEE/CVF Conference on Computer Vision and Pattern Recognition*, pages 6152–6162, 2020. 1, 3, 6
- [25] Jogendra Nath Kundu, Siddharth Seth, MV Rahul, Mugalodi Rakesh, Venkatesh Babu Radhakrishnan, and Anirban Chakraborty. Kinematic-structure-preserved representation for unsupervised 3d human pose estimation. In *Proceed-*

- ings of the AAAI Conference on Artificial Intelligence, pages 11312–11319, 2020. [1](#), [3](#), [6](#)
- [26] Yang Li, Kan Li, Shuai Jiang, Ziyue Zhang, Congzhen-tao Huang, and Richard Yi Da Xu. Geometry-driven self-supervised method for 3d human pose estimation. In *Proceedings of the AAAI Conference on Artificial Intelligence*, pages 11442–11449, 2020. [2](#)
- [27] Long Lian, Zhirong Wu, and Stella X Yu. Bootstrapping objectness from videos by relaxed common fate and visual grouping. In *Proceedings of the IEEE/CVF Conference on Computer Vision and Pattern Recognition*, pages 14582–14591, 2023. [3](#), [5](#)
- [28] Hongyi Liu and Lihui Wang. Collision-free human-robot collaboration based on context awareness. *Robotics and Computer-Integrated Manufacturing*, 67:101997, 2021. [1](#)
- [29] Hai Liu, Tingting Liu, Zhaoli Zhang, Arun Kumar Sangaiah, Bing Yang, and Youfu Li. Arhpe: Asymmetric relation-aware representation learning for head pose estimation in industrial human–computer interaction. *IEEE Transactions on Industrial Informatics*, 18(10):7107–7117, 2022. [1](#)
- [30] Matthew Loper, Naureen Mahmood, Javier Romero, Gerard Pons-Moll, and Michael J Black. Smpl: A skinned multi-person linear model. *ACM Transactions on Graphics*, 34(6): 1–16, 2015. [3](#), [4](#)
- [31] Dominik Lorenz, Leonard Bereska, Timo Milbich, and Bjorn Ommer. Unsupervised part-based disentangling of object shape and appearance. In *Proceedings of the IEEE/CVF Conference on Computer Vision and Pattern Recognition*, pages 10955–10964, 2019. [1](#), [2](#), [6](#)
- [32] Ali Ahmad Malik, Tariq Masood, and Arne Bilberg. Virtual reality in manufacturing: immersive and collaborative artificial-reality in design of human-robot workspace. *International Journal of Computer Integrated Manufacturing*, 33(1):22–37, 2020. [1](#)
- [33] Dushyant Mehta, Helge Rhodin, Dan Casas, Pascal Fua, Oleksandr Sotnychenko, Weipeng Xu, and Christian Theobalt. Monocular 3d human pose estimation in the wild using improved cnn supervision. In *3D Vision, 2017 Fifth International Conference on*. IEEE, 2017. [1](#), [2](#), [6](#), [7](#), [8](#)
- [34] Daniela Mihai and Jonathon Hare. Differentiable drawing and sketching. *arXiv preprint arXiv:2103.16194*, 2021. [4](#)
- [35] Alejandro Newell, Kaiyu Yang, and Jia Deng. Stacked hour-glass networks for human pose estimation. In *Computer Vision–ECCV 2016: 14th European Conference, Amsterdam, The Netherlands, October 11–14, 2016, Proceedings, Part VIII 14*, pages 483–499. Springer, 2016. [3](#)
- [36] Chuer Pan, Brian Okorn, Harry Zhang, Ben Eisner, and David Held. Tax-pose: Task-specific cross-pose estimation for robot manipulation. In *Conference on Robot Learning*, pages 1783–1792. PMLR, 2023. [1](#)
- [37] Sida Peng, Yuanqing Zhang, Yinghao Xu, Qianqian Wang, Qing Shuai, Hujun Bao, and Xiaowei Zhou. Neural body: Implicit neural representations with structured latent codes for novel view synthesis of dynamic humans. In *Proceedings of the IEEE/CVF Conference on Computer Vision and Pattern Recognition*, pages 9054–9063, 2021. [1](#)
- [38] Douglas A Reynolds et al. Gaussian mixture models. *Encyclopedia of biometrics*, 741(659-663), 2009. [5](#)
- [39] Helge Rhodin, Victor Constantin, Isinsu Katircioglu, Mathieu Salzmann, and Pascal Fua. Neural scene decomposition for multi-person motion capture. In *Proceedings of the IEEE/CVF Conference on Computer Vision and Pattern Recognition*, pages 7703–7713, 2019. [7](#)
- [40] Olaf Ronneberger, Philipp Fischer, and Thomas Brox. U-net: Convolutional networks for biomedical image segmentation. In *Medical Image Computing and Computer-Assisted Intervention–MICCAI 2015: 18th International Conference, Munich, Germany, October 5–9, 2015, Proceedings, Part III 18*, pages 234–241. Springer, 2015. [4](#)
- [41] Luca Schmidtko, Athanasios Vlontzos, Simon Ellershaw, Anna Lukens, Tomoki Arichi, and Bernhard Kainz. Unsupervised human pose estimation through transforming shape templates. In *Proceedings of the IEEE/CVF Conference on Computer Vision and Pattern Recognition*, pages 2484–2494, 2021. [2](#), [5](#), [6](#)
- [42] James A Sethian. Fast marching methods. *SIAM review*, 41(2):199–235, 1999. [5](#)
- [43] Sagar Sharma, Simone Sharma, and Anidhya Athaiya. Activation functions in neural networks. *Towards Data Sci*, 6(12):310–316, 2017. [4](#)
- [44] Aliaksandr Siarohin, Stéphane Lathuilière, Sergey Tulyakov, Elisa Ricci, and Nicu Sebe. First order motion model for image animation. *Advances in Neural Information Processing Systems*, 32, 2019. [1](#), [2](#)
- [45] Ashish Singh, Antonio Bevilacqua, Thach Le Nguyen, Feiyan Hu, Kevin McGuinness, Martin O’Reilly, Darragh Whelan, Brian Caulfield, and Georgiana Ifrim. Fast and robust video-based exercise classification via body pose tracking and scalable multivariate time series classifiers. *Data Mining and Knowledge Discovery*, 37(2):873–912, 2023. [1](#)
- [46] Jose Sosa and David Hogg. Self-supervised 3d human pose estimation from a single image. In *Proceedings of the IEEE/CVF Conference on Computer Vision and Pattern Recognition*, pages 4787–4796, 2023. [1](#), [3](#), [6](#), [7](#)
- [47] Chris Stauffer and W Eric L Grimson. Adaptive background mixture models for real-time tracking. In *Proceedings. 1999 IEEE Computer Society Conference on Computer Vision and Pattern Recognition (Cat. No PR00149)*, pages 246–252. IEEE, 1999. [3](#)
- [48] Jennifer J Sun, Lili Karashchuk, Amil Dravid, Serim Ryou, Sonia Fereidooni, John C Tuthill, Aggelos Katsaggelos, Bingni W Brunton, Georgia Gkioxari, Ann Kennedy, et al. Bkind-3d: Self-supervised 3d keypoint discovery from multi-view videos. In *Proceedings of the IEEE/CVF Conference on Computer Vision and Pattern Recognition*, pages 9001–9010, 2023. [1](#), [3](#), [6](#)
- [49] Xiao Sun, Bin Xiao, Fangyin Wei, Shuang Liang, and Yichen Wei. Integral human pose regression. In *Proceedings of the European Conference on Computer Vision*, pages 529–545, 2018. [3](#), [4](#)
- [50] Supasorn Suwajanakorn, Noah Snaveley, Jonathan J Tompson, and Mohammad Norouzi. Discovery of latent 3d keypoints via end-to-end geometric reasoning. *Advances in Neural Information Processing Systems*, 31, 2018. [3](#), [6](#)
- [51] James Thewlis, Samuel Albanie, Hakan Bilen, and Andrea Vedaldi. Unsupervised learning of landmarks by descrip-

- tor vector exchange. In *Proceedings of the IEEE/CVF International Conference on Computer Vision*, pages 6361–6371, 2019. [6](#)
- [52] Pekka J Toivanen. New geodesic distance transforms for gray-scale images. *Pattern Recognition Letters*, 17(5):437–450, 1996. [4](#)
- [53] Bastian Wandt, Marco Rudolph, Petrisa Zell, Helge Rhodin, and Bodo Rosenhahn. Canonpose: Self-supervised monocular 3d human pose estimation in the wild. In *Proceedings of the IEEE/CVF Conference on Computer Vision and Pattern Recognition*, pages 13294–13304, 2021. [2](#)
- [54] Jianbo Wang, Kai Qiu, Houwen Peng, Jianlong Fu, and Jianke Zhu. Ai coach: Deep human pose estimation and analysis for personalized athletic training assistance. In *Proceedings of the 27th ACM International Conference on Multimedia*, pages 374–382, 2019. [1](#)
- [55] Yuxin Wu and Kaiming He. Group normalization. In *Proceedings of the European Conference on Computer Vision*, pages 3–19, 2018. [6](#)
- [56] Wei Xu. Toward human-centered ai: a perspective from human-computer interaction. *Interactions*, 26(4):42–46, 2019. [1](#)
- [57] Zhenbo Yu, Bingbing Ni, Jingwei Xu, Junjie Wang, Chenglong Zhao, and Wenjun Zhang. Towards alleviating the modeling ambiguity of unsupervised monocular 3d human pose estimation. In *Proceedings of the IEEE/CVF International Conference on Computer Vision*, pages 8651–8660, 2021. [2](#)
- [58] Yuting Zhang, Yijie Guo, Yixin Jin, Yijun Luo, Zhiyuan He, and Honglak Lee. Unsupervised discovery of object landmarks as structural representations. In *Proceedings of the IEEE Conference on Computer Vision and Pattern Recognition*, pages 2694–2703, 2018. [1](#), [2](#), [6](#)

# Mask as Supervision: Leveraging Unified Mask Information for Unsupervised 3D Pose Estimation

## Supplementary Material

### A. Cascade Training

#### A.1. Auxiliary Loss

Apart from mask reconstruction loss in the Sec. 3.2, several auxiliary losses are introduced to strengthen the unsupervised system.

**Constant bone length loss.** Pre-define a list of bone lengths, including torso-pelvis, thorax-torso, neck-thorax, nose-neck, and head-nose, denoted as  $C$ . We utilize a sub-optimal loss to initialize a general skeleton.

$$L_{bone_c} = \lambda_{bone_c} \sum_b^B \|\mathbf{B}_b - C_b\|_2^2 \quad (12)$$

**Equivalence loss.** Same as [44], we expect keypoints with spatial invariance can be discovered. Let denote  $\mathcal{T}$  as a 2D affine transformation,  $\phi$  as our keypoint detector, and  $\mathbf{I}$  as the input image. The model is constrained to predict keypoints with equivalence constraints that enforce the commutativity of applying a transformation  $\mathcal{T}$  either before or after detection.

$$L_{eq} = \lambda_{eq} \sum_{i=0}^J \|\mathcal{T}(\phi(\mathbf{I})) - \phi(\mathcal{T}(\mathbf{I}))\|_2^2 \quad (13)$$

**Symmetry loss.** Considering the inner symmetry of the human skeleton, we leverage this prior to providing supervision. In detail, the shoulders and hips are bilaterally symmetrical to the thorax and pelvis, respectively. We denote  $\mathbf{x}_l$  and  $\mathbf{x}_r$  as the left and right side of endpoints,  $\mathbf{x}_c$  as symmetrical midpoints in 2D.

$$L_{sym} = \lambda_{sym} \|(\mathbf{x}_l + \mathbf{x}_r)/2 - \mathbf{x}_c\|_2^2 \quad (14)$$

#### A.2. Bone Mask.

As mentioned in the body structure prior, each bone mask  $\mathbf{B}_b$  is formally defined as

$$\mathbf{B}_b(\mathbf{x}) = \exp(-d_b^2(\mathbf{p}, \mathbf{x}(i_b), \mathbf{x}(j_b))/\sigma^2) \quad (15)$$

where  $\sigma$  is a hyper-parameter controlling bone width, and  $d_b$  is the  $L_2$  distance between pixel  $\mathbf{p}$  in the map and the line segment. Specifically, the distance  $d_b$  is defined as

$$d_b = \begin{cases} \|\mathbf{p} - \mathbf{x}(i_b)\|_2, & \text{if } r \leq 0 \\ \|\mathbf{p} - (\mathbf{x}(i_b) + r\mathbf{x}(j_b))\|_2, & \text{if } 0 < r < 1, \\ \|\mathbf{p} - \mathbf{x}(j_b)\|_2, & \text{if } r \geq 1, \end{cases} \quad (16)$$

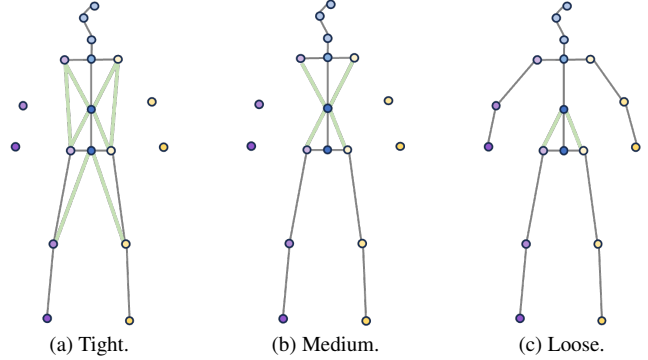


Figure 7. Schematic of different skeleton designs. Green lines indicate auxiliary connections for better mask fitting.

where,

$$r = \frac{(\mathbf{p} - \mathbf{x}(i_b)) \cdot (\mathbf{x}(i_b) - \mathbf{x}(j_b))}{\|\mathbf{x}(i_b) - \mathbf{x}(j_b)\|_2^2}. \quad (17)$$

#### A.3. Training Details

To gradually approach the ground truth and avoid numerous local optima in training, we design a cascade training procedure to disentangle bones. Different connections in the skeleton are demonstrated in Fig. 7.

For the first stage, we utilize the tight form to depict the skeleton mask  $\mathbf{M}_{Skel}$ . It selects dense connections in the torso and omits the connections at the arms since the main part shows less diversity which is beneficial for the model to warm up. In initialization, we first take the gravity centroid and a point with a fixed distance from the centroid as pseudo pairs to supervise the predicted pelvis and thorax for 400 steps. Following that, two pivotal joints are coarsely located. Meanwhile, Constant bone length loss  $L_{bone_c}$ , Equivalence loss  $L_{eq}$ , and Symmetry loss  $L_{sym}$  are adopted to assist the reconstruction of the skeleton mask  $L_{Skel}$ . In detail, we take  $\lambda_s = 10.0$  with geodesic weighting and 2.5, 1.0, 2.0 for  $\lambda_{bone_c}$ ,  $\lambda_{eq}$ ,  $\lambda_{sym}$  respectively. Note that  $\lambda_{bone_c}$  is a sub-optimal target, the given  $\lambda_{bone_c}$  will only generate a small loss in the order of  $1e-3$ . With geodesic weighting, the selected joints are progressively driven to ideal locations from the gathered. This procedure takes 15 epochs with a  $2e-4$  learning rate.

After the reconstruction loss in the skeleton mask meets convergence, we then adopt the physique mask  $\mathbf{M}_{Physo}$  to replenish mask representations. In this stage, we aim to train the Shape Prior Network  $\psi$  to drive the arm joints in the final stage. The medium form of the skeleton mask is

leveraged which contains fewer auxiliary connections and provides more flexibility in pose estimation. In terms of loss function, we remove the Constant bone length loss  $L_{bone_c}$  while keeping the Equivalence loss  $L_{eq}$  and Symmetry loss  $L_{sym}$ . To avoid the unexpected extension of shoulders (i.e. extend to the arms region), we remove the geodesic weighting for both the skeleton mask and physique mask and take 1.0 and 4.0 for  $\lambda_s$  and  $\lambda_p$ . Besides, we force both the left and the right hand, as well as the left and the right elbow, to be positioned in the same location. It eliminates bias between the left and right parts as an initialization for the last stage. Experimentally, we constrained it for the first 600 steps. The Shape Prior Network undertakes a simple task and converges fast in 5 epochs.

In the last stage, we fully utilize the proposed modules, including the skeleton mask, the physique mask, and geodesic weighting. The loose form opts to offer enough flexibility to estimate the locations of the arm parts. We keep the auxiliary loss in the second stage and take 2.0 and 1.5 for  $\lambda_s$  and  $\lambda_p$ . The entire framework is trained with a multi-step schedule that the learning rate starts at  $2e - 4$  for the first 14 epochs and decays to  $1e - 4$  for the next 11 epochs.

The bone width  $\sigma$  in the skeleton mask is set round  $3 \times 10^{-3}$  depending on different cascade periods. We use Adam optimizer [21] with a learning rate  $2 \times 10^{-4}$ . The network is trained 45 epochs in total with batch size 32. It takes about 9 hours on two 3090 GPUs.

## B. Ablation Study

In this section, we supplemented qualitative and quantitative results in the ablations study to further elaborate on the effectiveness of our proposed components.

### B.1. Skeleton mask as structural representation.

Note that our structure prior can degenerate into a Gaussian-like point-based representation. Therefore, with configuration hyperparams controlled, we practically implement the baseline method by taking joints and themselves as bone connections.

Table 5. Ablation study on the skeleton mask.  $\psi$ : shape prior network. SPP: supervised post-processing. We remove skeleton priors to demonstrate the consequences of the lack of structural information.

Configurations	2D MSE-% ( $\downarrow$ )
<i>wo structure prior, wo <math>\psi</math></i>	20.22
<i>wo structure prior</i>	20.06
<i>wo structure prior + SPP</i>	9.32
structure prior & $\psi$	3.63

The quantitative results in Tab. 5 demonstrate the effectiveness of structure prior and the utilities to alternate the supervised post-processing (SPP), which is compatible with the conclusion in Sec. 4.6. Formally, compared with the first two configurations, it indicates the structural prior is learned from our skeleton mask and the physique Mask will not provide structural information since the generator  $\psi$  treats all keypoints as equal. After adding the powerful but supervised SPP, the performance grows with the post-processing network learned from training poses. In the last line of configurations, with structure prior, the plausible skeletons can be constructed without supervision and present lower error.

### B.2. Physique Mask as Shape Representation.

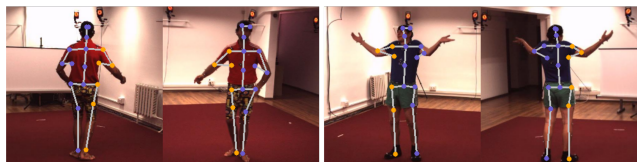


Figure 8. Visualizations of the configurations that remove shape prior network and geodesic weighting.

In Fig. 8, we visualize the results without shape prior network and geodesic weighting. It can be seen that keypoints are located in the main part of the body since the upper body shows larger spatial diversity causing problems in optimization. The Shape Prior Network  $\psi$  provides shape-level representations, requiring keypoints expansion as hints for a complete reconstructed mask and eventually drives keypoints to the extremities. Moreover, with the help of geodesic weighting, which constructs a smoother solution space and deals with corner cases, leading to further improved performance.